

Calcium mediated static and dynamic allosteric in S100A12: Implications for target recognition by S100 proteins

Qian Wang¹ | Christopher DiForte^{1,2} | Aleksey Aleshintsev^{1,2} | Gianna Elci¹ | Shibani Bhattacharya³  | Angelo Bongiorno^{1,2} | Rupal Gupta^{1,2} 

¹Department of Chemistry, College of Staten Island, City University of New York, New York, United States

²Ph.D. Programs in Biochemistry and Chemistry, The Graduate Center of the City University of New York, United States

³New York Structural Biology Center, New York, New York, United States

Correspondence

Rupal Gupta and Angelo Bongiorno,
Department of Chemistry, College of
Staten Island, The City University of New
York, USA.

Email: rupal.gupta@csi.cuny.edu and
angelo.bongiorno@csi.cuny.edu

Shibani Bhattacharya, New York
Structural Biology Institute, New York,
USA.

Email: sbhattacharya@nysbc.org

Funding information

National Institutes of Health; National
Science Foundation

Review Editor: Carol Beth Post

Abstract

Structure and functions of S100 proteins are regulated by two distinct calcium binding EF hand motifs. In this work, we used solution-state NMR spectroscopy to investigate the cooperativity between the two calcium binding sites and map the allosteric changes at the target binding site. To parse the contribution of the individual calcium binding events, variants of S100A12 were designed to selectively bind calcium to either the EF-I (N63A) or EF-II (E31A) loop, respectively. Detailed analysis of the backbone chemical shifts for wild-type protein and its mutants indicates that calcium binding to the canonical EF-II loop is the principal trigger for the conformational switch between ‘closed’ apo to the ‘open’ Ca^{2+} -bound conformation of the protein. Elimination of binding in S100-specific EF-I loop has limited impact on the calcium binding affinity of the EF-II loop and the concomitant structural rearrangement. In contrast, deletion of binding in the EF-II loop significantly attenuates calcium affinity in the EF-I loop and the structure adopts a ‘closed’ apo-like conformation. Analysis of experimental amide nitrogen (^{15}N) relaxation rates (R_1 , R_2 , and $^{15}\text{N}-\{^1\text{H}\}$ NOE) and molecular dynamics (MD) simulations demonstrate that the calcium bound state is relatively floppy with pico–nanosecond motions induced in functionally relevant domains responsible for target recognition such as the hinge domain and the C-terminal residues. Experimental relaxation studies combined with MD simulations show that while calcium binding in the EF-I loop alone does not induce significant motions in the polypeptide chain, EF-I regulates fluctuations in the polypeptide in the presence of bound calcium in the EF-II loop. These results offer novel insights into the dynamic regulation of target recognition by calcium binding and unravels the role of cooperativity between the two calcium binding events in S100A12.

Qian Wang, Christopher DiForte, and Aleksey Aleshintsev contributed equally to this study.

KEY WORDS

calcium binding proteins, molecular dynamics simulations, NMR spectroscopy, S100 proteins

1 | INTRODUCTION

Biological sensors such as proteins require controlled modulation of their structure and/or dynamics to execute cellular signaling. Such dynamic or static modulation of the conformational space often entails cooperative interactions between different domains of the polypeptide. S100 family of proteins are exemplary models of regulatory molecules that undertake distinct architectural transformation to achieve target specificity upon calcium binding (Donato et al., 2013; Foell et al., 2006). Albeit 25%–60% sequence similarity, each S100 protein exhibits unique target selectivity triggered by calcium binding, which allows these proteins to regulate a diverse array of intra- and extracellular activities. S100 proteins execute these functionalities with a pair of EF-hand motifs that assemble to form a four-helix bundle. The EF loop at the C-terminal (EF-II) is a canonical 12 residue motif found in all calcium binding proteins, while the N-terminal loop (EF-I), composed of 14 amino acids, is specific to the S100 family (Grabarek, 2006). This pseudo-EF loop is distinct from its canonical counterpart. Unlike the pentagonal bipyramidal Ca^{2+} coordination afforded by the sidechain carbonyl groups in the EF-II loop, binding of calcium ions in the EF-I loop takes place primarily via backbone carbonyl groups. While structurally distinct, the EF loops are spatially coupled allowing them to cooperatively regulate the structure and functions of S100 proteins (Szebenyi & Moffat, 1986). However, the contributions of the individual calcium binding domains and their extent in the exerted cooperativity is not fully understood. Furthermore, the functional relevance of biologically unique EF-I loop remains unclear.

Most S100 proteins exist as (homo)dimers, allowing them to ligate four calcium ions per dimeric unit. A hallmark of S100 proteins is the distinct conformational rearrangement upon calcium binding, which exposes a hydrophobic surface known to be the site of target binding (Nelson & Chazin, 1998a). Within the four-helix bundle, the EF-I loop tethers helices 1 and 2, while the EF-II loop connects helix 3 and 4. The linker connecting helix 2 and 3 or the so-called ‘hinge domain’ is the putative site for target binding in many S100 proteins. In calcium saturated state of S100 proteins, helix 3 undergoes a large reorientation compared to the apo protein, while the orientation of other helices remains relatively unchanged. Such independent reorganization of the different

domains is unique to the S100 family of proteins (Grabarek, 2006; Potts et al., 1995). Several seminal works in the literature have evaluated the cooperativity of calcium sequestration and the subsequent implications on structure and dynamics for some S100 and related proteins (Smith et al., 2012; Nelson & Chazin, 1998b; Immadisetty et al., 2021; Akke et al., 1993a; Inman et al., 2001; Pálfy et al., 2016; Akke et al., 1993b; Lee et al., 2000). So far we know that the high sequence and structural homology between the S100 family of proteins underlies a generic mechanism of function mediated by calcium binding, but the origin of the specificity of individual S100 proteins towards biological partners is not well understood. Analogous to other functionally versatile but sequentially conserved domains, the S100 family has also evolved unique mechanisms to expand the molecular recognition space (Lee et al., 2008; Bertini et al., 2013; Ecsédi et al., 2021; Wheeler & Harms, 2021).

S100A12, a homodimeric member of the S100 family, is responsible for both intra- and extracellular regulatory functions. In addition to calcium buffering, S100A12 also sequesters Zn^{2+} ions from invading pathogens in the extracellular milieu during infection (Donato et al., 2013; Goyette & Geczy, 2011; Cunden & Nolan, 2018; Zackular et al., 2015). Zn^{2+} and Ca^{2+} binding to this protein is cooperatively coupled, but the atomistic details of this cooperativity are currently not available (Dell'Angelica et al., 1994; Moroz et al., 2009b; Cunden et al., 2016). S100A12, with its Zn^{2+} sequestration mediated antimicrobial functions is a prominent member of the human innate immune response along with S100A8/A9 heterodimer. We have previously reported on structural characterization of divalent metal ion bound S100A12 (Wang et al., 2019), augmenting existing structural information on this protein (Moroz et al., 2001, 2002, 2003b, 2009a; Hung et al., 2013). Additionally, we have demonstrated that calcium binding mediates dynamic coupling between the two EF-loops in the micro-millisecond (μs - ms) timescale regime (Wang et al., 2022). Despite extensive characterization of the modular structure, parsing the contributions of the individual EF loops is challenging owing to the cooperativity between the EF loops.

Here, we evaluate the contributions of the individual EF-loops towards modulating the structure and dynamics of S100A12. NMR characterization of S100A12 variants that selectively bind to calcium in the EF-I or the EF-II loop demonstrate that the EF-II loop is the primary

determinant of the overall architecture of the protein upon calcium binding. High frequency fluctuations of the amide bond vectors probed using NMR relaxation measurements provide insights into site specific pico-nanosecond (ps-ns) timescale motions in the presence and absence of bound calcium. The results indicate that calcium binding regulates fluctuations in functionally relevant domains of the protein. Molecular dynamics (MD) simulations recapitulating the experimentally observed high frequency fluctuations enable estimation of conformations entropies originating from individual calcium binding events, thereby providing quantitative insights into the cooperativity exerted by the EF loops. These findings, in addition to providing atomistic consequences of calcium binding to S100A12, also provide clues into general mechanism of target recognition by S100 proteins.

2 | RESULTS

2.1 | Deletion of calcium binding in the EF-I loop

Calcium binds to the EF-I loop via backbone carbonyl groups of S18, K21, H23, and T26 and the sidechain carboxylate moiety of E31. Based on studies on the homologous protein S100B, we hypothesized that a single mutation at position 14 (E31A) may be sufficient to eliminate calcium binding in the EF-I loop (Markowitz et al., 2005). Calcium binding monitored by isothermal calorimetry (ITC) titrations revealed a single binding event for the E31A variant of S100A12 with a $K_D = 20 \pm 5 \mu\text{M}$, indicating that this mutation indeed eliminates binding to the EF-I loop while preserving calcium binding in the EF-II loop (Figure 1a). Dissociation constant for Ca^{2+} binding to the EF-II loop in S100 proteins typically range between 0.1 and 100 μM (Pietzsch & Hoppmann, 2009; Zimmer & Weber, 2010) and K_D of $\sim 50 \mu\text{M}$ has been reported for S100A12 extracted from pig granulocytes (Dell'Angelica et al., 1994). The relatively small variation in the Ca^{2+} binding affinity of E31A compared to the wildtype protein implies the cooperativity between the two sites has limited impact on the higher affinity site. Backbone chemical shift assignments were obtained from triple resonance experiments (3D HNCACB and CBCACONH) and 2D ^1H - ^{15}N HSQC experiments performed on uniformly ^{13}C - and ^{15}N -labeled apo and Ca^{2+} -E31A mutant proteins respectively. We successfully assigned 82/92 and 88/92 residues for both the apo- and the calcium bound proteins, respectively. NMR titration performed with the aid of these chemical shift assignments yielded a K_D value in

agreement with the ITC measurements ($K_D^{\text{NMR}} = 16 \pm 3 \mu\text{M}$; Figure 1b).

In the X-ray structure of the apo protein, the bidentate carboxylate group of E31 forms a hydrogen bond with a water molecule in the vacant N-terminal pseudo-EF loop and S28 hydroxyl group (PDB: 2WCE) (Moroz et al., 2009a). The residue specific profile of the ^1H , ^{15}N chemical shift perturbations (CSPs) suggests the point mutation rearranges the configuration of the EF-I loop but the helical core of the protein is still intact when compared to the wildtype apo-protein (Figures 1c and S1a). Residue specific plots between backbone amide nitrogen (^{15}N) and proton (^1H) chemical shifts of apo-wildtype and E31A proteins exhibits a near perfect correlation, suggesting that the mutation does not alter the overall architecture of the protein (Figure 1c). The perturbation of multiple residues (55–75, 85–90) in the C-terminal EF-II domain (Figure 1c) in the mutated protein is consistent with strong coupling between the metal binding sites in the apo state (Wang et al., 2022).

Unlike the wildtype protein where both EF loops are functional, the addition of calcium is expected to disproportionately affect residues in the EF-II loop from the mutated protein. This assumption is validated by the large deviations observed ($> 1 \text{ ppm}$) for residues 25–37 in the EF-I loop and not the EF-II loop in E31A compared to the wild-type protein (Figure 1d). This is attributed to the difference between the metal free state in E31A versus Ca^{2+} coordination by EF-I in the wildtype protein. In the absence of significant CSPs at residues (except E72) in the EF-II loop directly involved in coordinating the Ca^{2+} ion, we conclude the canonical binding mode is not impacted adversely by the remodeling of the EF-I loop. The cumulative chemical shift change in each EF loop is sensitive not only to the coordination of Ca^{2+} ion, but also to the extent of coupling between the loops in different coordination states. Therefore, in E31A, calcium binding in EF-II is expected to perturb some residues (25–35) in the metal free EF-I loop as seen in Figure S1b. Conversely, the difference in the CSPs of residues 68–70 in the Ca^{2+} bound EF-II loop (Figure 1d) indicates the vacant EF-I loop interacts differently with the metal bound EF-II loop in the half-saturated state of E31A. We note that the observed chemical shift changes cannot be attributed to inter-subunit CSP effects because the Ca^{2+} binding sites are $\sim 12 \text{ \AA}$ apart in the dimeric structure. In both apo- and Ca^{2+} -E31A, backbone chemical shift analysis by TALOS (Figure S1) shows the secondary structure in the two EF-hands is not influenced by the mutation in the EF-I loop. Additionally, residue specific backbone amide chemical shifts of apo and Ca^{2+} bound wildtype and E31A proteins are highly correlated,

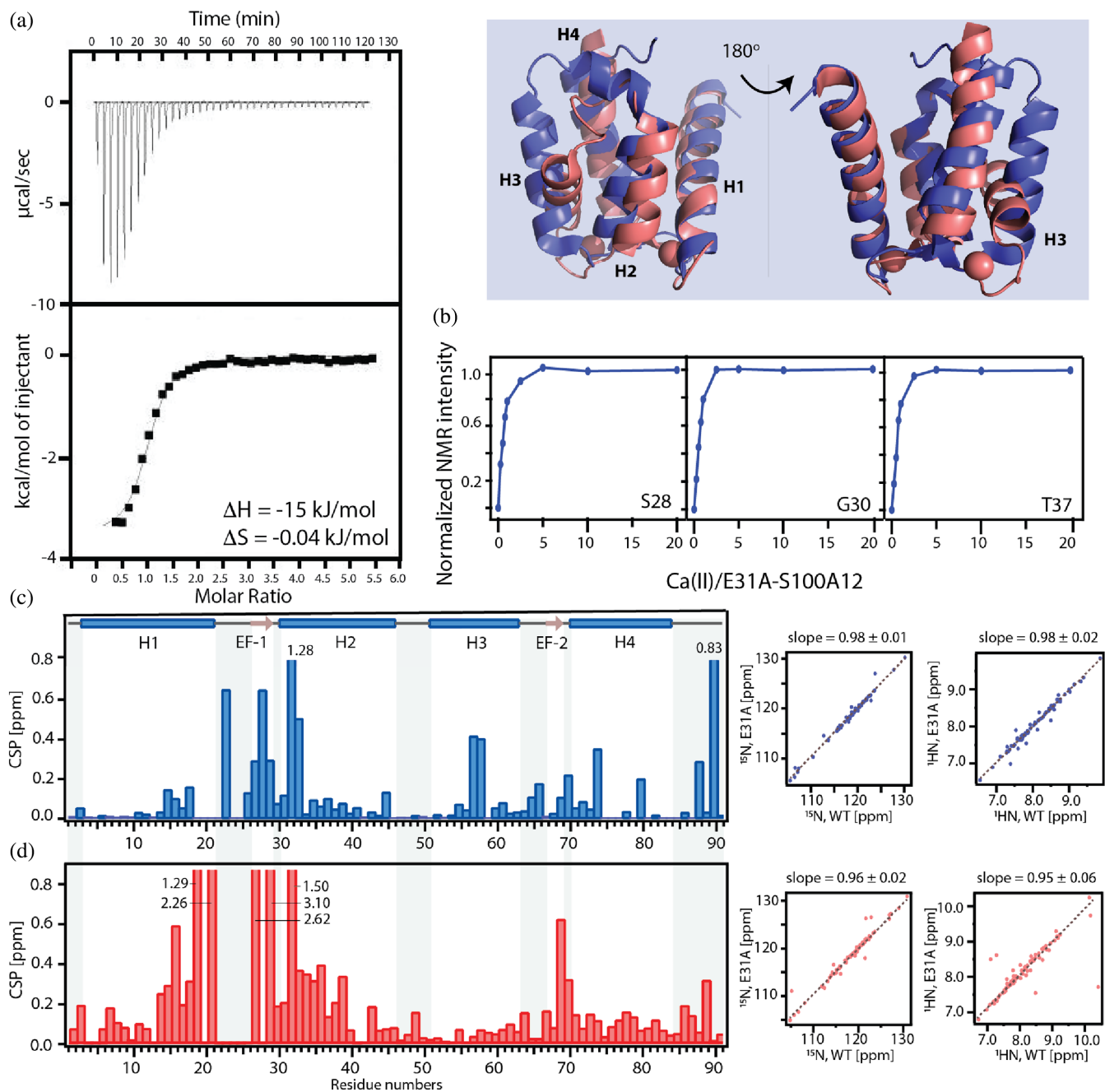


FIGURE 1 Calcium binding to the E31A variant of S100A12. (a) Normalized change in heat versus equivalents of calcium added to E31A mutant obtained from ITC, (b) normalized peak intensities for select residues during calcium titration to E31A and site-specific weighted ^1H , ^{15}N CSPs (left) and the correlation between ^1H and $^{15}\text{N}^{\text{H}}$ chemical shifts (right) between wildtype and E31A proteins in the absence (c) and presence (d) of calcium. An overlay of the crystal structures of apo (PDB: 2WCF) and calcium bound (PDB: 1E8A) S100A12 showing the reorientation of helix 3 (H3) upon calcium binding is shown in the top-right inset. Only one subunit of the dimer is shown for clarity.

suggesting high degree of structural similarity (Figure 1d). Thus, structurally, the half-saturated state of E31A mutant adopts a conformation closer to the fully saturated Ca^{2+} -bound state of the wildtype protein. To further decouple the role of the two metal binding loops, we generated a complementary mutation which eliminated Ca^{2+} binding exclusively in the EF-II loop.

2.2 | Deletion of calcium binding in the EF-II loop

Calcium binding in the 12 residue canonical EF-II loop primarily takes place via sidechain carbonyl groups (Moroz et al., 2003a) and mutating any of the positions has a drastic effect on Ca^{2+} binding affinity (Liriano

et al., 2012). In the EF-II loop of S100A12, D61, N63, D65, Q67, D69, and E72 are involved in calcium binding. Given the proximity of D61 and E72 to the termini of helix 3 and 4 respectively, these residues were considered unsuitable as candidates for mutation. A better option was the highly conserved asparagine at position 3 in the EF-II loop, with a flexible sidechain in the apo protein. Therefore, with the goal of eliminating Ca^{2+} binding with marginal impact on the protein structure, we selected the N63A mutation for further characterization by NMR. The ^1H - ^{15}N HSQC spectra of apo N63A and the wildtype protein are nearly superimposable (Figure S2a) which facilitated the assignment of 78/91 backbone amide resonances. The ^1H , ^{15}N CSPs displayed in Figure 2a indicate the most significant changes map to the EF-II loop (>0.2 ppm) compared to minor changes in the remaining protein. Like the E31A mutation, remote perturbation in N63A confirms the presence of interactions between the EF-hand domains (Figure 2a). Two key observations from calcium titrations on N63A include: (i) unlike the wildtype and E31A proteins, high concentrations of calcium (~ 100 equivalents) were required to fully saturate the protein, and (ii) in the presence of a large excess of calcium, N63A is structurally similar to the apo state (Figure 2b) and the backbone resonances deviate significantly from the wild type Ca^{2+} bound protein in both EF-hands (Figure 2c). The largest CSPs in the C-terminal EF hand (helix 3 and helix 4; Figure 2b) can be attributed to Ca^{2+} binding in the mutated protein. NMR titrations monitoring changes in chemical shifts provide an estimated Ca^{2+} binding affinity of ~ 35 mM at the EF-I binding site (Figure S2b) which is more than an order of magnitude weaker than the native protein (0.1–1 mM; Figure S5).

To summarize, the structural comparison between the two mutations and their calcium dependent conformational response presents strong evidence for cooperative interaction between the two sites where the higher affinity EF-II loop is essential for enabling Ca^{2+} binding in the EF-I loop. Secondly, the calcium induced conformational switch in the C-terminal EF-hand required for ligand interaction is triggered primarily by Ca^{2+} binding in the canonical EF-II loop while binding in the EF-I loop has marginal impact on the activation of the protein (Figure 2c).

2.3 | Picosecond to nanosecond motions in wildtype S100A12

Motions of the backbone amide N–H bond vectors in picosecond–nanosecond (ps–ns) timescale were probed

by $^{15}\text{N}^{\text{H}}$ longitudinal (R_1), transverse (R_2) spin relaxation rates and, steady-state nuclear Overhauser enhancements ($^{15}\text{N}-\{^1\text{H}\}$ NOE) for apo and calcium bound S100A12. Backbone resonance assignments of these forms of the protein have been previously reported (Wang et al., 2019; Hung et al., 2013). With the aid of these assignments, 86 out of 91 resonances in the apo and 83 resonances in the calcium bound protein can be unambiguously assigned in the 2D ^1H - ^{15}N correlation spectra of relaxation measurements. The cross-peaks assigned to functionally important residues in the canonical EF-II loop (11, apo; 11: Ca^{2+} bound) and the hinge region (16, apo; 15, Ca^{2+} bound out of 16) exhibited adequate signal-to-noise for data analysis. Owing to severe exchange broadening the data for only a subset of residues in the S100 specific EF-I loop (9, apo; 2, Ca^{2+} bound) were analyzed. R_1 , R_2 , R_2/R_1 , and NOE versus residue numbers for both states of the protein are presented in Tables S2 and S3. Motional parameters for each state were determined with the extended Lipari–Szabo model-free formalism (Lipari & Szabo, 1982a, 1982b) implemented in the Relax software (d’Auvergne & Gooley, 2008a, 2008b) from data acquired at two fields, 11.7 T (apo, Ca^{2+}), 18.8 T (Ca^{2+}), and 21.1 T (apo), respectively.

2.3.1 | Apo protein

Relaxation analysis for 15 out of 91 amino acids could not be performed either due to weak or overlapping peak intensities in the 2D ^1H - ^{15}N planes. Most of these residues belong to the EF-I loop and EF-II loops. The average values of the generalized order parameter, S^2_{avg} , for the entire polypeptide chain was 0.83, indicating that the protein backbone is generally rigid. The hinge domain, EF-II and the C-terminal region of the protein exhibit small fluctuations in the ps–ns timescale regime while the rest of the polypeptide remains relatively rigid. The available order parameters for residues in the EF-I suggest that the N-terminal S100 specific loop is more rigid than the canonical EF-II loop (Table S1 and Figure 3). The calculations show that except for the C-terminal, majority of residues undergoing motions such as in the hinge domain and the EF-II loop, exhibit internal correlation times, $\tau_e < 100$ ps (Figure 3b).

2.3.2 | Ca^{2+} -S100A12

Optimized motional parameters for calcium bound S100A12 were similar to that of the apo protein as determined by the averaged order parameters of the four

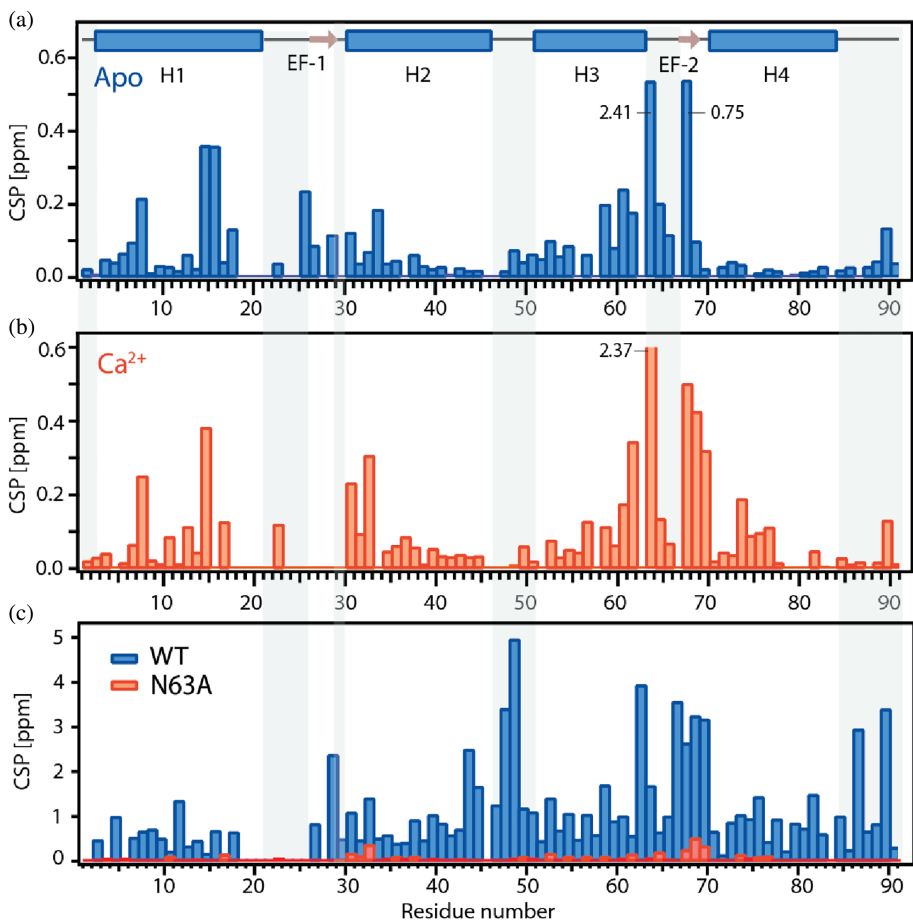


FIGURE 2 Site-specific weighted ^1H - ^{15}N CSPs between apo-wildtype and (a) apo N63A, (b) Ca^{2+} -N63A. (c) Site specific chemical shift perturbations between apo and calcium bound wildtype (blue) and N63A (orange) proteins.

helices ($S^2_{\text{helix1}} = 0.86 \pm 0.04$, $S^2_{\text{helix2}} = 0.85 \pm 0.05$, $S^2_{\text{helix3}} = 0.84 \pm 0.04$, and $S^2_{\text{helix4}} = 0.87 \pm 0.03$). Figure 3a shows a comparison of the order parameters of apo and calcium bound protein. While order parameters for most residues in the EF-I loops are not available, motions in the EF-II loop were attenuated upon calcium binding. In contrast to the EF loops, calcium binding manifests elevated motions in the C-terminal residues. Unequivocal increase in backbone fluctuations were monitored for C-terminal residues such as H85 and T88 in the presence of calcium. Interestingly in the hinge domain, the N-terminal residues experience increased mobility (E39, L40, I44, and N46), while the C-terminal residues become more rigid (K48, K50, and I53) with the notable exception of A51 and V52. As shown in Figure 3b, overall, the fast timescale motions (<50 ps) detected in the hinge domain, EF-II loop and the C-terminal backbone are comparable to similar amplitude motions in the apo protein. However, unlike the apo protein, significantly slower sub-nanosecond motions ~ 500 ps (τ_s) were identified exclusively in the Ca^{2+} bound protein (Figure 3c). These much slower timescale motions (~ 500 ps) identified in the hinge domain and C-terminal residues are broadly consistent with

conformational fluctuations between the calcium bound ‘open’ structures but absent in the ‘closed’ apo state.

2.4 | Comparison of faster timescale motions in wildtype and mutants

It is well established that the variation in the heteronuclear ^1H - ^{15}N NOEs correlates with the dynamic trends represented by the S^2 values (Figure S3). Therefore, to evaluate the role of dynamics in the cooperative interaction between the EF loops we measured the backbone amide ^1H - ^{15}N NOEs for apo and Ca^{2+} bound E31A and N63A mutants. A comparison of site-specific ^1H - ^{15}N NOEs of apo and Ca^{2+} bound proteins is shown in Figure 4. Overall, the helices and the Ca^{2+} loops are less flexible compared to the hinge region and the C-terminal residues. In the wildtype protein, the already dynamic C-terminal increases further in flexibility upon Ca^{2+} binding along with the hinge region linking the two EF hand domains (Figure 3). This enhanced mobility at the principal ligand binding surface (Xie et al., 2007) appears to be finely tuned by the ability to bind Ca^{2+} at one or both EF loops. For instance, in E31A with Ca^{2+} bound at

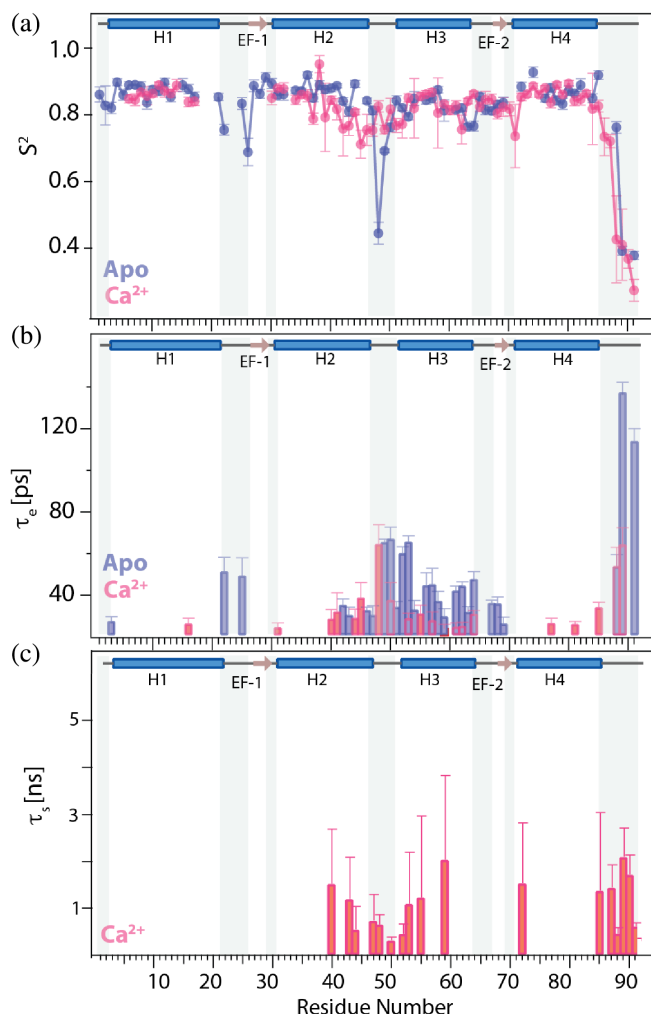


FIGURE 3 (a) and (b) Site-specific generalized order parameter, S^2 (filled circles) and τ_e (bars) for apo (blue) and calcium bound (red) S100A12. (c) Residue-wise internal correlation times at slower timescales, τ_s , for Ca^{2+} -S100A12.

the EF-II loop, the dynamic response is very similar to the wildtype protein in contrast to the absence of change in N63A where the EF-II loop is functionally defective. Collectively, the dynamics agrees with the conclusions drawn from the chemical shift analysis of the mutants, which showed the importance of the coordination state of the EF-II loop in mediating the conformational transformation of the protein.

2.5 | MD simulations of S100A12 and its variants

To gain further insight into the conformational space of the different metal ligated states, we performed MD simulations of apo and calcium bound forms of wildtype and E31A S100A12 proteins. Owing to the structural perturbation introduced by the E31A mutation in both EF-hand

domains (Figure 1c) we also performed MD simulations on a half-saturated state of wildtype S100A12 bearing Ca^{2+} only in the EF-II loop (Ca^{2+} (EF-II)-S100A12). Apo and Ca^{2+} bound wildtype proteins maintained their structural integrity throughout the 0.5 μs simulations. Order parameters were determined from these MD trajectories using variable averaging times ranging between 100 ps and 10 ns. As shown in Figure 5a,c, S^2 values derived from the shorter averaging times of ca. 500 ps are in better agreement with the experimental data compared to longer times. These results are also in agreement with model-free calculations yielding τ_e and τ_s of ca. 100 ps and 2 ns, respectively (Figure 3b,c). MD derived S^2 values recapitulate motions in the C-terminal tail and the hinge domain (residue 38–52), while reproducing the overall rigidity of the remaining helices. Additionally, the simulations exhibit the expected trend of dampening of motions in the EF loops upon calcium binding.

Given the excellent correlation between experimental and theoretical S^2 values, we turned our attention to E31A model structure loaded with calcium in both EF loops. Within the first 50 ns of the trajectory, the calcium ions in the EF-I loop were released to the water environment, in agreement with our experimental data demonstrating that E31A mutation inhibits calcium binding to the EF-I loop. Subsequent MD simulations were performed on E31A and the wildtype proteins with calcium bound to the EF-II loop only. In these simulations, the calcium ions remained in the EF-II loop throughout the trajectory for both proteins with the structural integrity of the protein preserved throughout the simulation. For E31A, the NMR chemical shifts predicted using ShiftX (Han et al., 2011) on the structure extracted from this MD trajectory are in reasonable agreement with experimental values when compared to the predicted chemical shifts for the wildtype protein (Figure S4), suggesting that the overall architecture of MD equilibrated structure is in agreement with the protein in solution observed by NMR. The order parameters derived from these simulations are presented in Figure 5b. As expected, the EF-I loop shows greater mobility, similar to the apo-wild type protein. Furthermore, the C-terminal tail shows depressed S^2 values, consistent with the dip in the experimentally observed NOE data for the mutant reflecting a highly flexible backbone.

2.6 | Evaluating the entropic contribution to calcium binding affinity

The change in the conformational entropy derived from generalized order parameters offers a powerful approach to parse residue specific contributions to the free energy of binding ligands (Jarymowycz & Stone, 2006). A

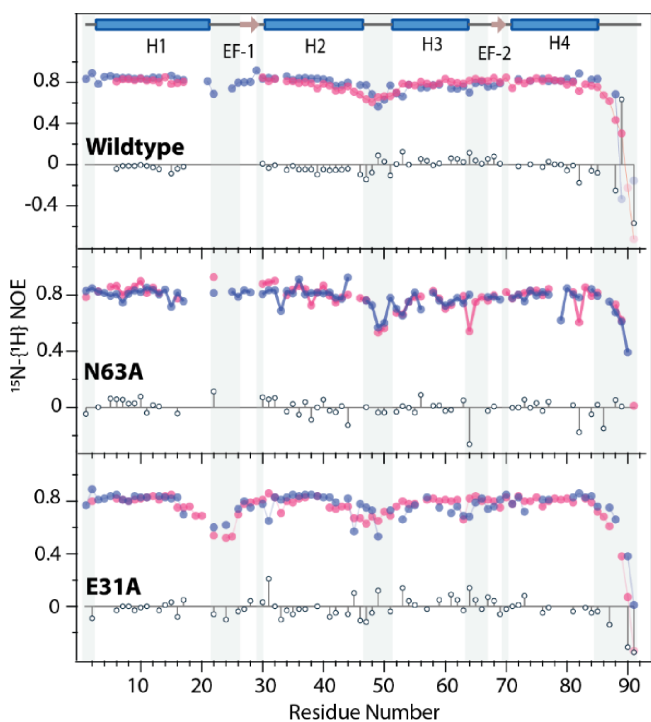


FIGURE 4 Site-specific $\{{}^1\text{H}\}-{}^{15}\text{N}$ NOEs for apo (blue) and calcium bound (pink) S100A12 proteins acquired at 25°C and 11.7 T. For clarity, difference in NOE values between the calcium bound and apo states are shown as sticks in each panel.

pertinent application of this methodology quantified the entropic contributions of individual calcium binding EF loops and showed synergistic binding between EF-I and II loops in calbindin D_{9k} (Akke et al., 1993a; Akke et al., 1993b; Linse & Chazin, 1995; Wimberly et al., 1995). These works utilized the (Cd^{2+})₁ state as a proxy for calcium binding to the EF-II loop and a mutant (N56A) to enable binding exclusively in the EF-I loop (Wimberly et al., 1995). By measuring the binding affinities between the apo, two half-saturated (Cd^{2+} at site 2 and Ca^{2+} at site 1) and the doubly (Ca^{2+})₂ saturated states (Akke et al., 1993b; Linse & Chazin, 1995), the authors were able to demonstrate that the dominant contribution of the free energy comes from Ca^{2+} binding to the EF-II loop (Akke et al., 1993b; Linse & Chazin, 1995). As an extension to these previous works, below we have quantified the entropic contributions of the individual EF loops towards the overall conformational entropy of S100A12.

Instead of considering the experimental amide bond order parameters, the present analysis relies on calculating change in conformational entropy (ΔS) using order parameters derived from the MD trajectories. Given the excellent agreement in the trend between experimentally measured and MD derived S^2 values for the wildtype protein (Figure 5), the use of the MD results for our analysis

bears some benefits. For instance, we can sample the order parameters of residues not amenable to direct observation by NMR owing to extensive exchange broadening in the calcium binding loops. Also, by comparing the MD derived entropic changes in the calcium binding loops between the apo, half and fully saturated states, we can parse the contributions of individual calcium binding events.

Our analysis rests on the assumption that the calcium binding events occur sequentially, first to the EF-II and then to the EF-I loop. The half-saturated state, resulting from the binding of calcium to the EF-II loop, can be modeled either by $\text{Ca}^{2+}(\text{EF-II})-\text{S100A12}$ or $\text{Ca}^{2+}-\text{E31A}$. While the half-saturated state represented by the E31A mutant is experimentally amenable, the overall conformational space of this protein may also be influenced by the mutation, as evident from the observed CSPs. In this scenario, the MD analysis considering the half saturated state as $\text{Ca}^{2+}-\text{E31A}$ would account for both the calcium binding events and perturbations introduced by the mutation. Since these two effects are entangled, here we focus on ΔS occurring along the apo $\rightarrow \text{Ca}^{2+}(\text{EF-II})-\text{S100A12} \rightarrow \text{Ca}^{2+}-\text{S100A12}$ pathway in Table 1 and the results obtained for the E31A pathway are reported in Table S4.

The ΔS analysis of our MD derived order parameters, based on the formalism developed by Kay and coworkers (Yang et al., 1997), shows that the two calcium binding events induce distinct domain-dependent changes in the conformational entropy of S100A12 (ΔG_c). The coordination of the first Ca^{2+} ion leads to a significant loss in conformational entropy in the EF-II loop but increases floppiness in (almost) all the other domains, including the EF-I loop and the putative target binding hinge domain. The net free energy change (-9.4 kJ/mol) is negative, indicating that the first binding event to the high affinity EF-II loop is enthalpically driven (Figure 1a) with favorable entropic contributions. In contrast, the second binding event leads to significant entropy losses in all domains, except in helix 1 and C-terminal, amounting to an overall free energy penalty of 28.1 kJ/mol. Notably the coordination of Ca^{2+} ion to the EF-I loop has marginal effect on the dynamics in the EF-II loop.

In the alternate pathway involving the E31A mutation, similar trends are observed in the entropic contributions to the free energy calculated for EF-II, C-terminal, and hinge domains. The first calcium binding causes the configurational entropy to increase in both the EF-II and EF-I loops, leading to an overall increase of the configurational free energy by about 9 kJ/mol. The second binding event affects mostly the mobility of helix 3; it leads to almost no conformational entropy changes in the EF-I loop but

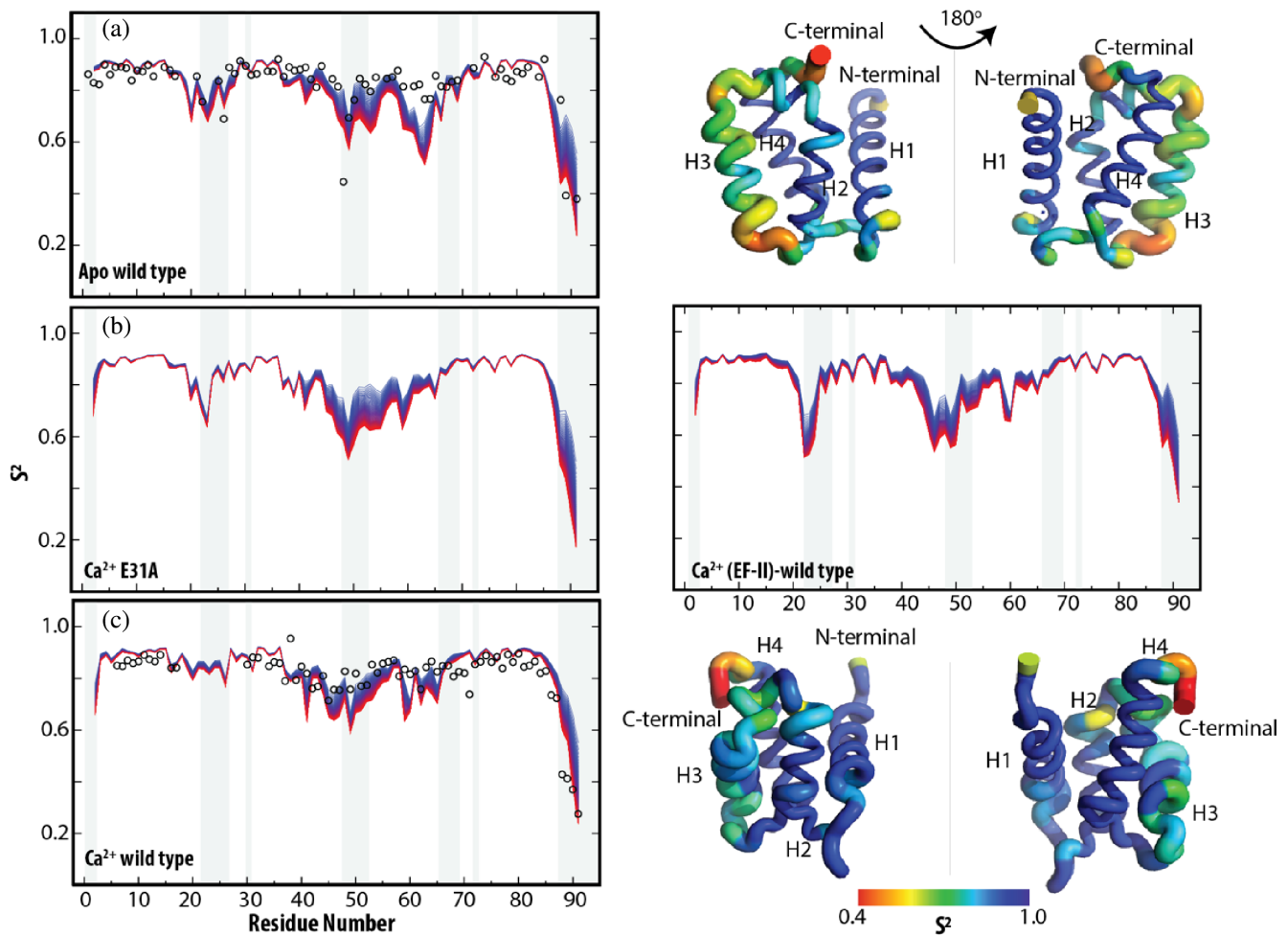


FIGURE 5 Site-specific generalized order parameter computed from 0.5 μ s MD trajectories with variable averaging time windows (from 100 ps; blue – 10 ns; red) for (a) apo S100A12; (b) Ca^{2+} -E31A (left) and Ca^{2+} -(EF-II)-S100A12 (right) and; (c) Ca^{2+} -S100A12. Experimental model-free S^2 values are shown in open circles. The worm representation of the backbone shows the S^2 values (top: apo; bottom: Ca^{2+} -S100A12) mapped on the structure of the protein with the radius of the tube proportional to the timescale of motion (only the monomeric chain is shown for the sake of clarity).

increases the mobility of EF-II. Consequently, the summation of the configurational free energy increases by 9 kJ/mol. Key takeaways from all these results are: (i) the dynamics of the calcium binding loops are strongly correlated where binding to the EF-II loop modulates the dynamics of the EF-I loop and vice versa, and (ii) calcium binding in the EF-II loop increases the entropy of the hinge domain and the C-terminal residues which may facilitate optimal target interaction. Despite the possibility of the influence of the mutation in E31A, we can draw similar conclusions from the data related to these key conformational changes in the loop and target binding site, which reinforces the functionally calibrated dynamic response triggered by the two calcium binding events. Overall, both sets of entropy changes derived by considering either the half-saturated state of S100A12 or the mutant as intermediate states between apo and

Ca^{2+} -S100A12 indicate that the two calcium binding events are correlated, and they induce striking dynamical changes throughout the whole protein.

3 | DISCUSSION

The characterization of S100A12 and its variants described here demonstrates that the two EF loops bind Ca^{2+} cooperatively with long-range effect on the structure and dynamics of the protein. To evaluate the extent of cooperativity between the two EF loops we have used a combination of NMR, ITC, and MD simulations to characterize the half and fully saturated states of the protein. In biological milieu, the high affinity EF-II loop in the S100 proteins binds Ca^{2+} with $K_D \approx 0.1\text{--}100 \mu\text{M}$, while the EF-I loop exhibits a lower Ca^{2+} affinity ranging between 0.1 and 1 mM (Pietzsch & Hoppmann, 2009).

TABLE 1 Change in conformational entropy (in J/K/mol) for domains of S100A12.

	$\Delta S^{\text{II apo}} \rightarrow \text{Ca}^{2+}(\text{EF-II})$	$\Delta S^{\text{II,I Ca}^{2+}(\text{EF-II}) \rightarrow \text{Ca}^{2+}\text{-S100A12}}$	$\Delta G_c = -T\Delta S^{\text{TOT}}$
Helix 1	11.1 (-3.3)	7.4 (-2.2)	-5.5
EF-I	15.3 (-4.6)	-53.0 (15.8)	11.2
Helix 2	9.3 (-2.8)	-10.6 (3.2)	0.4
Hinge	31.8 (-9.5)	-25.0 (7.5)	-2.0
Helix 3	-3.4 (1.0)	-11.0 (3.3)	4.3
EF-II	-48.5 (14.5)	-2.0 (0.6)	15.1
Helix 4	9.9 (-3.0)	-10.3 (3.1)	0.1
C-terminal	5.6 (-1.7)	10.8 (-3.2)	-4.9

Note: The last column gives values of $\Delta G_c = -T\Delta S^{\text{TOT}}$ at 298 K (in of kJ/mol), ΔS values are reported in the units of J/K/mol; $-T\Delta S$ values at 298 K are presented parentheses in the units of kJ/mol.

The distinct binding affinities of the two EF loops are key to the biological functions of S100 proteins, particularly in the cytoplasm. Typical basal Ca^{2+} concentrations ($\sim 100 \text{ nM}$) are not sufficient to fully saturate the EF loops of cytosolic S100 proteins, many of which are present in micromolar concentrations. This prevents the depletion of free Ca^{2+} ions in the intercellular space. The activation of S100 proteins is regulated by a spike in the intracellular Ca^{2+} levels ($\sim 500 \text{ nM}$) in concert with enhanced target association initiating specific cellular response (Young et al., 2022). This activation mechanism has been characterized for several S100 proteins such as S100A1, S100B and S100A4 (Malashkevich et al., 2008; Wright et al., 2005, 2009; Prosser et al., 2008; Charpentier et al., 2010; Rustandi et al., 1998; Garrett et al., 2008; Duelli et al., 2014). For S100A12, while modulation of calcium sequestration upon target binding as not been established, several intracellular target proteins have been identified (Hatakeyama et al., 2004). An understanding of Ca^{2+} modulated structural and dynamical attributes of S100A12 is therefore needed for evaluating the interdependence of S100A12-target interaction and calcium binding.

The point mutations E31A (EF-I) and N63A (EF-II) have vastly different effects on Ca^{2+} binding affinity and the accompanying conformational changes in the protein. The loss of Ca^{2+} binding in the EF-I loop has marginal effect on suppressing calcium binding in the canonical EF-II motif ($K_D \sim 20 \mu\text{M}$) compared to the wild-type protein. This result is contrary to previously reported studies on S100B where the E31A mutation completely abrogates binding in the EF-II loop (Markowitz et al., 2005). The N63A mutant, which lacks the ability to bind calcium in the EF-II loop, exhibits significantly lower affinity ($\sim 35 \text{ mM}$) than expected from the pseudo loop (0.1–1 mM, Figure S5), hinting at the presence of positive cooperativity between the two

binding sites. The more than two orders of magnitude difference in the Ca^{2+} binding affinities in the two EF loops in S100A12 implies sequential binding starting with the saturation of the EF-II site before the second EF-I site is fully occupied. Therefore, any positive cooperativity is expected to enhance the affinity at the EF-I site once the EF-II loop is saturated with calcium. This conclusion is in general agreement with other multi-step calcium binding proteins like the N-terminal domain of Calmodulin and Calbindin D_{9k} (Linse & Chazin, 1995; Beccia et al., 2015).

The coupling of low and high affinity Ca^{2+} binding sites is the structural foundation of the dual functionality of S100s as Ca^{2+} sensors in cell signaling (EF-II) and homeostasis of metal ions (EF-I) (Donato et al., 2013). The entropy calculations reveal the tentative mechanism of a feedback loop whereby reduced mobility of the Ca^{2+} bound EF-II loop modulates the dynamics of the EF-I loop and the target binding site both of which become more malleable. While the conformational flexibility in the structure aids target selectivity it can also reduce Ca^{2+} affinity by increasing the entropic cost of rearranging the binding loops. However, one could argue that once the higher affinity EF-II site is occupied, the solvent exposed target binding site is poised for binding the target. It is likely that the subsequent rigidification of the structure (Liriano et al., 2012) in the target bound state plays an important role in shifting the equilibrium of the dynamic ensemble in favor of better-defined structures which could lower the entropic penalty for Ca^{2+} binding at both loops. This is also consistent with the results from the MD simulations of the wild-type protein which indicate Ca^{2+} bound EF-I loop makes the backbone more rigid. The role of target mediated conformational dynamics in tuning calcium affinities is an open question for S100A12 and a topic for future studies.

The major structural differences between apo and Ca^{2+} -S100A12 originates from the reorientation of helix 3 triggered by calcium binding in EF-II loop. Based on chemical shift data (Figure 2), the N63A mutation favors a conformation like the apo protein both in the absence and presence of calcium. In apo-E31A protein, we see the evidence of local conformational changes in the EF-I loop propagated to helix 1. Because EF-I and EF-II loops are coupled, the C-terminal EF-hand domain also undergoes some rearrangement in the apo state. Except for the binding loops, the calcium bound state is indistinguishable from the wild-type protein in the C-terminal EF-hand domain. As seen in the X-ray structures of S100A12 with different coordination states and by NMR in this study, the N-terminal EF hand has limited conformational flexibility. In contrast, in the C-terminal EF-hand both NMR chemical shifts and MD simulations revealed an ‘open’ to ‘close’ conformational switch driven primarily by calcium binding to EF-II loop. This raises an important question, whether the difference in the calcium dependent response of the EF hands is encoded by the intrinsic flexibility of the loop sequence or dictated by the stability of the helical motif. There is some evidence from calbindin D_{9k}, a member of the S100 family, that showed replacing EF-I with EF-II loop failed to modify the response of N-terminal domain (Malmendal et al., 1998). Thus, the activation of the S100s is tunable not just by modulating the Ca^{2+} binding affinity but the dynamic response depends on the rigidity of the hydrophobic core.

In addition to introducing structural modifications, calcium binding to S100A12 also influences internal dynamics of the polypeptide. Barring the EF-II loop, the relatively rigid apo protein presents a stark contrast to the dynamic allosteric detected in the calcium bound state of the protein. The rigidification of the EF-II loop in the Ca^{2+} bound state causes increased backbone mobility at the target binding site formed by the C-terminal and hinge region of the protein on the faster timescale. The presence of fast timescale (ps-ns) motions in several S100 and related proteins has been evaluated in the literature (Akke et al., 1993b; Inman et al., 2001; Pálfy et al., 2016; Koerdel et al., 1992; Dutta et al., 2008; Nowakowski et al., 2013; Spyracopoulos et al., 1998; Gagné et al., 1998). Generally, the C-terminal domain in S100B, S100A4, S100A1, calbindin D_{9k}, and troponin have been shown to be flexible in the fast timescale regime, which is allosterically coupled to Ca^{2+} binding. This plasticity at the binding site is not only vital for targeting multiple binding partners (Bhattacharya et al., 2004), but plays a key role in the synchronization of Ca^{2+} uptake and release linked with target association and dissociation in signaling (Wang et al., 2022; Rustandi et al., 1998; Zhang et al., 2017).

The findings of this work reinforce major conclusions drawn from a common paradigm of calcium mediated function of S100 family of proteins. The remarkable similarity of the proteins presents a challenge to understand how each member fine tunes its function for different signaling pathways. All S100 protein undergo a structural rearrangement upon calcium binding driven primarily driven by EF-II loop. The significance of the EF-I loops, and its marginal impact on the conformational changes in the protein is less understood. In this study, we have decoded the cascade of dynamic changes triggered by the simple act of calcium binding in the loops. Thus, the local entropy of C-terminal residues at the binding site increases with near equal contributions from both calcium binding events. However, the hinge domain experiences opposing contributions from the two binding events resulting in overall a modest increase in the conformation entropy of this critical region in the fully calcium saturated state. Being the putative target binding sites, such complementary changes in the backbone dynamics may be a key component of molecular recognition: whereby the mobility of the C-terminal domain could facilitate ligand binding via the classical induced fit model and, restricted motions in the hydrophobic hinge domain could impart some degree of target specificity. Like calmodulin and its many homologues, such dual mechanism is very effectively employed in the conformational selection of diverse targets (Westerlund & Delemotte, 2018) in signaling pathways without enabling promiscuous association.

In summary, in this report we evaluate the individual and cooperative contributions of the EF loops towards modulating the structure and dynamics of S100A12. The conformational transformation of the protein is not an isolated event dominated by calcium binding to the canonical EF-II loop but part of a cascade of structural and dynamic changes involving the pseudo-EF loop and the target binding site that are all coupled by a single signal. Despite the rigidity of the N-terminal domain and much lower calcium affinity, the EF-I loop is equally relevant and plays a critical supporting role in modulating the response of the canonical EF-hand domain.

4 | METHODS

4.1 | Protein expression and purification

Unenriched, ¹⁵N and ¹⁵N, ¹³C labeled recombinant wild-type was expressed and purified as previously reported (Wang et al., 2019). Single point mutagenesis to generate the E31A and N63A mutants was accomplished by polymerase chain reaction with the following primers: E31A

forward 5'- AAAGGCGCACTGAAACAGCTGCTG; E31A reverse: 5'-TTTCAGTGCAGCCTTGCTCAGCGT; N63A forward 5'-GGATGCGGCCAGGACGAACAAGTG; N63A reverse 5'-CCTGGGCCGATCCAGACCCTG. The identity of the plasmid upon mutagenesis was confirmed by DNA sequencing. The mutant plasmids were transformed into *Escherichia coli* BL21(DE3) cells. The mutants were expressed and purified using the same protocol as for the wildtype protein. For preparation of NMR samples, purified ^{15}N - or ^{13}C , ^{15}N labeled proteins were concentrated to 0.3–1 mM in aqueous buffer containing 20 mM MES (pH 6.0), 100 mM sodium chloride, 10% D₂O, and 200 mM 4,4-dimethyl-4-silapentane-1-sulfonic acid (DSS). Typical protein concentration for NMR measurements varied in the range of 300–800 μM . Ca²⁺ bound wildtype and E31A samples were prepared by adding 20 equivalents of Ca²⁺ to the protein. Ca²⁺-N63A was generated by adding 100 equivalents of calcium to the protein.

4.2 | Isothermal titration calorimetry

Isothermal titration calorimetry (ITC) experiments were conducted using a MicroCal VNP-200 titration calorimeter, measuring at 25°C. Both the protein samples and the concentrated calcium ions were dissolved in the buffer solution (20 mM HEPES at pH 7, 100 mM sodium chloride). The protein concentration in the reaction chamber was adjusted to 300 μM . During the experiment, calcium, serving as the ligand, was introduced into the system at 3-min intervals. A total of 40 injections were administered within a 120-min timeframe. Each injection consisted of 2 μL of solution, except for the initial injection, which utilized a volume of 0.3 μL . Numerical fitting of the data was performed using Origin software and associated macros provided by the manufacturer.

4.3 | NMR spectroscopy

NMR measurements were conducted on Bruker 500 MHz Ultrashield and 800 MHz US² spectrometers equipped with 5 mm TXI and 5 mm TCI CryoProbe, respectively. 2D $^1\text{H} - ^{15}\text{N}$ HSQC (Cavanagh et al., 2007) and three-dimensional (3D) $^1\text{H} - ^{15}\text{N} - ^{13}\text{C}$ CBCACONH (Grzesiek & Bax, 1992a, 1992b) experiments for resonance assignments were performed at 11.7 T and 37°C, while NMR titrations employed via $^1\text{H} - ^{15}\text{N}$ HSQC experiment were performed at 25°C. The laboratory frame R_1 , R_2 , and $^{15}\text{N}-\{^1\text{H}\}$ NOE relaxation spectra on apo (11.7 and 21.1 T) and Ca²⁺ bound (11.7 and 18.8 T) wildtype protein was recorded at two static fields and

37°C sample temperature according to established methods (Farrow et al., 1994). The pseudo 3D experiments were acquired with variable relaxation delays for $\text{N}^{15}-R_1$ ($\sim 0, 80, 200 \times 3, 400, 600, 800$, and 1000 ms) and $\text{N}^{15}-R_2$ (0.0, 16, 32 $\times 3$, 48, 64, 80, 96, and 128 ms) measurements. The heteronuclear $^{15}\text{N}-\{^1\text{H}\}$ NOE experiments were acquired with 4 s saturation plus 1 s recycle delay and the reference experiment with 5 s recycle delay. Each experiment was repeated two to three times to get an estimate of the standard deviation. The two-dimensional datasets were processed in NMRPipe (Delaglio et al., 1995), and the relaxation rates extracted from the mono-exponential decay of the intensity using rate analysis tools in NmrViewJ 8.0.3 (Johnson, 2004). The R_1 and R_2 data at high field (21.1 T) was scaled to account for small temperature offset from data acquired at lower field (11.7 T) (Gill et al., 2016). Experimentally obtained relaxation parameters at both magnetic fields are reported in Appendix S1. The field dependent relaxation rates were analyzed in the RELAX 4.0.3 program (d'Auvergne & Gooley, 2008a, 2008b) using the extended model-free formalism (Lipari & Szabo, 1982a, 1982b; Chen & Tjandra, 2008). Owing to exchange broadening in the calcium binding loops and the presence of sub-nanosecond motions, the data was best fitted with a local diffusion model (Schurr et al., 1994). The amide nitrogen relaxation rates measured for each residue at two fields are fit up to 10 different motional model, with and without slow exchange (R_{ex}) contribution to $^{15}\text{N}-R_2$ on the micro-millisecond timescales. The dynamic model that best fits the experimental data is selected based on Akaike information criterion (AIC) implemented in RELAX 4.0.3. The results of the best fitted model for each residue are summarized in Figure 3. For the two mutants $^{15}\text{N}-\{^1\text{H}\}$ NOE relaxation spectra on apo and Ca²⁺ bound state was acquired at a single static field (11.7 T) and 37°C sample temperature. The corresponding spectra were processed using the same methodology as described for the wildtype protein.

4.4 | MD simulations

MD simulations were carried out using the GROMACS software package (version 2022.3) (Abraham et al., 2015). Atomistic models of S100A12 homodimers were constructed based on the PDB files 1GQM (calcium-bound, chains G and H) and 2WCF (calcium-free, chains A and B). S100A12 variants was obtained from the PDB file 1GQM, after replacing the amino acid E31 with alanine. Protonation states of titratable residues were assigned based on pK_a values assuming pH 6.0. In particular, the protonation state of the histidine residues in each

symmetric chain of the homodimer was assigned according to the previous experimental findings (Wang et al., 2020), that is, His6 (neutral), His15 (protonated), His23 (neutral), His85 (protonated), His87 (protonated), and His89 (protonated). Each protein was inserted in a cubic box whose dimensions were determined by imposing a buffer width of 15 Å. The protein was then solvated in explicit water and neutralized by adding sodium and chlorine ions to have a concentration of 0.15 M. Overall, the atomistic models considered in this study encompassed 66,357 (calcium-bound), 58,802 (apo), and 69,372 (mutation) atoms. We used the AMBER99SB force field (Hornak et al., 2006) to describe proteins and ions, and the TIP3P model (Jorgensen et al., 1983) to treat the water environment. The systems were equilibrated at 300 K and 1 atm using standard procedures (Wang et al., 2022). After the equilibration step, the production run consisted of a MD simulation of 0.5 μs in the NPT ensemble at 300 K and 1 atm. MD simulations were carried out by using a time step of 2 fs using the particle mesh Ewald summation method with a grid spacing of 1.6 Å to calculate electrostatic interactions, the modified Berendsen thermostat to control the temperature, and the Parrinello–Rahman barostat to control the hydrostatic pressure. Bonds involving H atoms were constrained using the LINCS algorithm.

To calculate the order parameters (S^2) of the backbone amide bonds, we relied on the Lipari–Szabo model-free approach (Lipari & Szabo, 1982a) and adopted the truncated average approximation (Bowman, 2016):

$$S^2 = \frac{1}{\tau} \int_{\tau_m}^{\tau_m + \tau} C(t) dt,$$

where $C(t)$ is the angular correlation function describing the rotational dynamics of a N–H bond, τ_m is the isotropic rotational correlation time, and τ is 1 ns (Bowman, 2016). For completeness, we remark that $C(t)$ is calculated as follows:

$$C(t) = \langle P_2(\hat{\mu}(0) \cdot \hat{\mu}(t)) \rangle = \frac{1}{t_{MD} - t} \int_0^{t_{MD} - t} P_2(\hat{\mu}(\tau) \cdot \hat{\mu}(t + \tau)) d\tau$$

where $\hat{\mu}$ is the unit vector pointing along the N–H bond, $P_2(x) = (3x^2 - 1)/2$ is the second Legendre polynomial, and t_{MD} is the temporal length of the MD simulation.

AUTHOR CONTRIBUTIONS

Rupal Gupta: Conceptualization; investigation; funding acquisition; writing – original draft; writing – review and editing; formal analysis; data curation; supervision; project administration. **Qian Wang:** Conceptualization; data

curation; formal analysis. **Christopher DiForte:** Conceptualization; formal analysis; data curation. **Aleksey Alekhnitsev:** Conceptualization; formal analysis; data curation. **Gianna Elci:** Data curation; formal analysis. **shibani bhattacharya:** Conceptualization; writing – original draft; writing – review and editing; formal analysis; supervision; data curation. **Angelo Bonfiglio:** Conceptualization; funding acquisition; writing – original draft; writing – review and editing; formal analysis; supervision.

ACKNOWLEDGMENTS

This work was supported by the National Institutes of Health (GM131338-02) to R. G. NMR data presented herein were collected at the New York Structural Biology Institute (NYSBC). This work was performed in collaboration with the Center on Macromolecular Dynamics by NMR Spectroscopy (CoMD/NMR) at the NYSBC and supported by the U.S. National Institutes of Health (P41 GM118302). MD simulations were conducted with computational resources supported by the National Science Foundation Grant OAC-2215760. We thank Professor Brian Gibney at Brooklyn College for the access to ITC instrumentation.

ORCID

Shibani Bhattacharya  <https://orcid.org/0000-0002-7706-9167>

Rupal Gupta  <https://orcid.org/0000-0001-8637-6129>

REFERENCES

- Abraham MJ, Murtola T, Schulz R, Páll S, Smith JC, Hess B, et al. GROMACS: high performance molecular simulations through multi-level parallelism from laptops to supercomputers. SoftwareX. 2015;1–2:19–25. <https://doi.org/10.1016/j.softx.2015.06.001>
- Akke M, Brueschweiler R, Palmer AG III. NMR order parameters and free energy: an analytical approach and its application to cooperative calcium²⁺ binding by calbindin D9k. J Am Chem Soc. 1993b;115(21):9832–3. <https://doi.org/10.1021/ja00074a073>
- Akke M, Skelton NJ, Kordel J, Palmer AG III, Chazin WJ. Effects of ion binding on the backbone dynamics of calbindin D9k determined by nitrogen-¹⁵NMR relaxation. Biochemistry. 1993a; 32(37):9832–44. <https://doi.org/10.1021/bi00088a039>
- Beccia MR, Sauge-Merle S, Lemaire D, Brémont N, Pardoux R, Blangy S, et al. Thermodynamics of calcium binding to the calmodulin N-terminal domain to evaluate site-specific affinity constants and cooperativity. J Biol Inorg Chem. 2015;20(5):905–19. <https://doi.org/10.1007/s00775-015-1275-1>
- Bertini I, Borsi V, Cerofolini L, Das Gupta S, Fragai M, Luchinat C. Solution structure and dynamics of human S100A14. J Biol Inorg Chem. 2013;18(2):183–94. <https://doi.org/10.1007/s00775-012-0963-3>

- Bhattacharya S, Bunick CG, Chazin WJ. Target selectivity in EF-hand calcium binding proteins. *Biochim Biophys Acta*. 2004;1742(1–3):69–79. <https://doi.org/10.1016/j.bbamcr.2004.09.002>
- Bowman GR. Accurately modeling nanosecond protein dynamics requires at least microseconds of simulation. *J Comput Chem*. 2016;37(6):558–66. <https://doi.org/10.1002/jcc.23973>
- Cavanagh J, Fairbrother WJ, Palmer AG I, Rance M, Skelton NJ. Protein NMR spectroscopy – principles and practice. San Diego, CA: Academic Press; 2007.
- Charpentier TH, Thompson LE, Liriano MA, Varney KM, Wilder PT, Pozharski E, et al. The effects of CapZ peptide (TRTK-12) binding to S100B–Ca²⁺ as examined by NMR and X-ray crystallography. *J Mol Biol*. 2010;396(5):1227–43. <https://doi.org/10.1016/j.jmb.2009.12.057>
- Chen K, Tjandra N. Extended model free approach to analyze correlation functions of multidomain proteins in the presence of motional coupling. *J Am Chem Soc*. 2008;130(38):12745–51. <https://doi.org/10.1021/ja803557t>
- Cunden LS, Gaillard A, Nolan EM. Calcium ions tune the zinc-sequestering properties and antimicrobial activity of human S100A12. *Chem Sci*. 2016;7(2):1338–48. <https://doi.org/10.1039/C5SC03655K>
- Cunden LS, Nolan EM. Bioinorganic explorations of Zn(II) sequestration by human S100 host-defense proteins. *Biochemistry*. 2018;57(11):1673–80. <https://doi.org/10.1021/acs.biochem.7b01305>
- d'Auvergne EJ, Gooley PR. Optimisation of NMR dynamic models II. A new methodology for the dual optimisation of the model-free parameters and the Brownian rotational diffusion tensor. *J Biomol NMR*. 2008a;40(2):121–33. <https://doi.org/10.1007/s10858-007-9213-3>
- d'Auvergne EJ, Gooley PR. Optimisation of NMR dynamic models I. Minimisation algorithms and their performance within the model-free and Brownian rotational diffusion spaces. *J Biomol NMR*. 2008b;40(2):107–19. <https://doi.org/10.1007/s10858-007-9214-2>
- Delaglio F, Grzesiek S, Vuister GW, Zhu G, Pfeifer J, Bax A. NMRPipe: a multidimensional spectral processing system based on UNIX pipes. *J Biomol NMR*. 1995;6(3):277–93.
- Dell'Angelica EC, Schleicher CH, Santomé JA. Primary structure and binding properties of calgranulin C, a novel S100-like calcium-binding protein from pig granulocytes. *J Biol Chem*. 1994;269(46):28929–36. [https://doi.org/10.1016/S0021-9258\(19\)61996-4](https://doi.org/10.1016/S0021-9258(19)61996-4)
- Donato R, Cannon BR, Sorci G, Riuzzi F, Hsu K, Weber DJ, et al. Functions of S100 proteins. *Curr Mol Med*. 2013;13(1):24–57.
- Duelli A, Kiss B, Lundholm I, Bodor A, Petoukhov MV, Svergun DI, et al. The C-terminal random coil region tunes the Ca²⁺-binding affinity of S100A4 through conformational activation. *PLoS One*. 2014;9(5):e97654. <https://doi.org/10.1371/journal.pone.0097654>
- Dutta K, Cox CJ, Basavappa R, Pascal SM. ¹⁵N relaxation studies of apo-Mts1: a dynamic S100 protein. *Biochemistry*. 2008;47(29):7637–47. <https://doi.org/10.1021/bi8005048>
- Ecsédi P, Gógl G, Nyitrai L. Studying the structures of relaxed and fuzzy interactions: the diverse world of S100 complexes. *Front Mol Biosci*. 2021;8:749052. <https://doi.org/10.3389/fmolb.2021.749052>
- Farrow NA, Muhandiram R, Singer AU, Pascal SM, Kay CM, Gish G, et al. Backbone dynamics of a free and a phosphopeptide-complexed Src homology 2 domain studied by ¹⁵N NMR relaxation. *Biochemistry*. 1994;33(19):5984–6003. <https://doi.org/10.1021/bi00185a040>
- Foell D, Wittkowski H, Vogl T, Roth J. S100 proteins expressed in phagocytes: a novel group of damage-associated molecular pattern molecules. *J Leukoc Biol*. 2006;81(1):28–37. <https://doi.org/10.1189/jlb.0306170>
- Gagné SM, Tsuda S, Spyropoulos L, Kay LE, Sykes BD. Backbone and methyl dynamics of the regulatory domain of troponin C: anisotropic rotational diffusion and contribution of conformational entropy to calcium affinity. *J Mol Biol*. 1998;278(3):667–86. <https://doi.org/10.1006/jmbi.1998.1723>
- Garrett SC, Hodgson L, Rybin A, Toutchkine A, Hahn KM, Lawrence DS, et al. A biosensor of S100A4 metastasis factor activation: inhibitor screening and cellular activation dynamics. *Biochemistry*. 2008;47(3):986–96. <https://doi.org/10.1021/bi7021624>
- Gill ML, Byrd RA, Palmer AG III. Dynamics of GCN4 facilitate DNA interaction: a model-free analysis of an intrinsically disordered region. *Phys Chem Chem Phys*. 2016;18(8):5839–49. <https://doi.org/10.1039/C5CP06197K>
- Goyette J, Geczy CL. Inflammation-associated S100 proteins: new mechanisms that regulate function. *Amino Acids*. 2011;41(4):821–42. <https://doi.org/10.1007/s00726-010-0528-0>
- Grabarek Z. Structural basis for diversity of the EF-hand calcium-binding proteins. *J Mol Biol*. 2006;359(3):509–25. <https://doi.org/10.1016/j.jmb.2006.03.066>
- Grzesiek S, Bax A. Correlating backbone amide and side chain resonances in larger proteins by multiple relayed triple resonance NMR. *J Am Chem Soc*. 1992a;114(16):6291–3. <https://doi.org/10.1021/ja00042a003>
- Grzesiek S, Bax A. An efficient experiment for sequential backbone assignment of medium-sized isotopically enriched proteins. *J Magn Reson*. 1992b;99(1):201–7. [https://doi.org/10.1016/0022-2364\(92\)90169-8](https://doi.org/10.1016/0022-2364(92)90169-8)
- Han B, Liu Y, Ginzinger SW, Wishart DS. SHIFTX2: significantly improved protein chemical shift prediction. *J Biomol NMR*. 2011;50(1):43–57. <https://doi.org/10.1007/s10858-011-9478-4>
- Hatakeyama T, Okada M, Shimamoto S, Kubota Y, Kobayashi R. Identification of intracellular target proteins of the calcium-signaling protein S100A12. *Eur J Biochem*. 2004;271(18):3765–75. <https://doi.org/10.1111/j.1432-1033.2004.04318.x>
- Hornak V, Abel R, Okur A, Strockbine B, Roitberg A, Simmerling C. Comparison of multiple Amber force fields and development of improved protein backbone parameters. *Proteins*. 2006;65(3):712–25. <https://doi.org/10.1002/prot.21123>
- Hung K-W, Hsu C-C, Yu C. Solution structure of human Ca²⁺-bound S100A12. *J Biomol NMR*. 2013;57(3):313–8. <https://doi.org/10.1007/s10858-013-9781-3>
- Immadisetty K, Sun B, Kekenes-Huskey PM. Structural changes beyond the EF-hand contribute to apparent calcium binding affinities: insights from parvalbumins. *J Phys Chem B*. 2021;125(24):6390–405. <https://doi.org/10.1021/acs.jpcb.1c01269>
- Inman KG, Baldissari DM, Miller KE, Weber DJ. Backbone dynamics of the calcium-signaling protein apo-S100B as determined by ¹⁵N NMR relaxation. *Biochemistry*. 2001;40(12):3439–48. <https://doi.org/10.1021/bi0027478>

- Jarymowycz VA, Stone MJ. Fast time scale dynamics of protein backbones: NMR relaxation methods, applications, and functional consequences. *Chem Rev.* 2006;106(5):1624–71. <https://doi.org/10.1021/cr040421p>
- Johnson BA. Using NMRView to visualize and analyze the NMR spectra of macromolecules. *Methods Mol Biol.* 2004;278:313–52. <https://doi.org/10.1385/1-59259-809-9:313>
- Jorgensen WL, Chandrasekhar J, Madura JD, Impey RW, Klein ML. Comparison of simple potential functions for simulating liquid water. *J Chem Phys.* 1983;79(2):926–35. <https://doi.org/10.1063/1.445869>
- Koerdel J, Skelton NJ, Akke M, Palmer AG III, Chazin WJ. Backbone dynamics of calcium-loaded calbindin D9k studied by two-dimensional proton-detected nitrogen-15 NMR spectroscopy. *Biochemistry.* 1992;31(20):4856–66. <https://doi.org/10.1021/bi00135a017>
- Lee Y-T, Dimitrova YN, Schneider G, Ridenour WB, Bhattacharya S, Soss SE, et al. Structure of the S100A6 complex with a fragment from the C-terminal domain of Siah-1 interacting protein: a novel mode for S100 protein target recognition. *Biochemistry.* 2008;47(41):10921–32. <https://doi.org/10.1021/bi801233z>
- Lee AL, Kinnear SA, Wand AJ. Redistribution and loss of side chain entropy upon formation of a calmodulin–peptide complex. *Nat Struct Biol.* 2000;7(1):72–7. <https://doi.org/10.1038/71280>
- Linse S, Chazin WJ. Quantitative measurements of the cooperativity in an EF-hand protein with sequential calcium binding. *Protein Sci.* 1995;4(6):1038–44. <https://doi.org/10.1002/pro.5560040602>
- Lipari G, Szabo A. Model-free approach to the interpretation of nuclear magnetic resonance relaxation in macromolecules. 1. Theory and range of validity. *J Am Chem Soc.* 1982a;104(17):4546–59. <https://doi.org/10.1021/ja00381a009>
- Lipari G, Szabo A. Model-free approach to the interpretation of nuclear magnetic resonance relaxation in macromolecules. 2. Analysis of experimental results. *J Am Chem Soc.* 1982b;104(17):4559–70. <https://doi.org/10.1021/ja00381a010>
- Liriano MA, Varney KM, Wright NT, Hoffman CL, Toth EA, Ishima R, et al. Target binding to S100B reduces dynamic properties and increases Ca²⁺-binding affinity for wild type and EF-hand mutant proteins. *J Mol Biol.* 2012;423(3):365–85. <https://doi.org/10.1016/j.jmb.2012.07.011>
- Malashkevich VN, Varney KM, Garrett SC, Wilder PT, Knight D, Charpentier TH, et al. Structure of Ca²⁺-bound S100A4 and its interaction with peptides derived from nonmuscle myosin-IIA. *Biochemistry.* 2008;47(18):5111–26. <https://doi.org/10.1021/bi702537s>
- Malmendal A, Carlström G, Hamraeus C, Drakenberg T, Forsén S, Akke M. Sequence and context dependence of EF-hand loop dynamics. An ¹⁵N relaxation study of a calcium-binding site mutant of calbindin D9k. *Biochemistry.* 1998;37(8):2586–95. <https://doi.org/10.1021/bi971798a>
- Markowitz J, Rustandi RR, Varney KM, Wilder PT, Udan R, Wu SL, et al. Calcium-binding properties of wild-type and EF-hand mutants of S100B in the presence and absence of a peptide derived from the C-terminal negative regulatory domain of p53. *Biochemistry.* 2005;44(19):7305–14. <https://doi.org/10.1021/bi050321t>
- Moroz OV, Antson AA, Dodson EJ, Burrell HJ, Grist SJ, Lloyd RM, et al. The structure of S100A12 in a hexameric form and its proposed role in receptor signalling. *Acta Crystallogr Sect D.* 2002;58(3):407–13. <https://doi.org/10.1107/S0907444901021278>
- Moroz OV, Antson AA, Grist SJ, Maitland NJ, Dodson GG, Wilson KS, et al. Structure of the human S100A12–copper complex: implications for host–parasite defence. *Acta Crystallogr Sect D.* 2003b;59(5):859–67. <https://doi.org/10.1107/S0907444903004700>
- Moroz OV, Antson AA, Murshudov GN, Maitland NJ, Dodson GG, Wilson KS, et al. The three-dimensional structure of human S100A12. *Acta Crystallogr Sect D.* 2001;57(1):20–9. <https://doi.org/10.1107/S090744490001458X>
- Moroz OV, Blagova EV, Wilkinson AJ, Wilson KS, Bronstein IB. The crystal structures of human S100A12 in apo form and in complex with zinc: new insights into S100A12 oligomerisation. *J Mol Biol.* 2009a;391(3):536–51. <https://doi.org/10.1016/j.jmb.2009.06.004>
- Moroz OV, Burkitt W, Wittkowski H, He W, Ianoul A, Novitskaya V, et al. Both Ca²⁺ and Zn²⁺ are essential for S100A12 protein oligomerization and function. *BMC Biochem.* 2009b;10(1):11. <https://doi.org/10.1186/1471-2091-10-11>
- Moroz OV, Dodson GG, Wilson KS, Lukanidin E, Bronstein IB. Multiple structural states of S100A12: a key to its functional diversity. *Microsc Res Tech.* 2003a;60(6):581–92. <https://doi.org/10.1002/jemt.10300>
- Nelson MR, Chazin WJ. Structures of EF-hand Ca²⁺–binding proteins: diversity in the organization, packing and response to Ca²⁺ binding. *Biometals.* 1998a;11(4):297–318. <https://doi.org/10.1023/A:1009253808876>
- Nelson MR, Chazin WJ. An interaction-based analysis of calcium-induced conformational changes in Ca²⁺ sensor proteins. *Protein Sci.* 1998b;7(2):270–82. <https://doi.org/10.1002/pro.5560070206>
- Nowakowski M, Ruszczyńska-Bartnik K, Budzińska M, Jaremko Ł, Jaremko M, Zdanowski K, et al. Impact of calcium binding and thionylation of S100A1 protein on its nuclear magnetic resonance-derived structure and backbone dynamics. *Biochemistry.* 2013;52(7):1149–59. <https://doi.org/10.1021/bi3015407>
- Pálfy G, Kiss B, Nyitrai L, Bodor A. Multilevel changes in protein dynamics upon complex formation of the calcium-loaded S100A4 with a nonmuscle myosin IIA tail fragment. *Chembiochem.* 2016;17(19):1829–38. <https://doi.org/10.1002/cbic.201600280>
- Pietzsch J, Hoppmann S. Human S100A12: a novel key player in inflammation? *Amino Acids.* 2009;36(3):381–9. <https://doi.org/10.1007/s00726-008-0097-7>
- Potts BCM, Smith J, Akke M, Macke TJ, Okazaki K, Hidaka H, et al. The structure of calcyclin reveals a novel homodimeric fold for S100 Ca²⁺-binding proteins. *Nat Struct Biol.* 1995;2(9):790–6. <https://doi.org/10.1038/nsb0995-790>
- Prosser BL, Wright NT, Hernández-Ochoa EO, Varney KM, Liu Y, Olojo RO, et al. S100A1 binds to the calmodulin-binding site of ryanodine receptor and modulates skeletal muscle excitation–contraction coupling. *J Biol Chem.* 2008;283(8):5046–57. <https://doi.org/10.1074/jbc.M709231200>
- Rustandi RR, Drohat AC, Baldisseri DM, Wilder PT, Weber DJ. The Ca²⁺-dependent interaction of S100B(ββ) with a peptide

- derived from p53. *Biochemistry*. 1998;37(7):1951–60. <https://doi.org/10.1021/bi972701n>
- Schurr JM, Babcock HP, Fujimoto BS. A test of the model-free formulas. Effects of anisotropic rotational diffusion and dimerization. *J Magn Reson B*. 1994;105(3):211–24. <https://doi.org/10.1006/jmrb.1994.1127>
- Smith DMA, Straatsma TP, Squier TC. Retention of conformational entropy upon calmodulin binding to target peptides is driven by transient salt bridges. *Biophys J*. 2012;103(7):1576–84. <https://doi.org/10.1016/j.bpj.2012.08.037>
- Spryacopoulos L, Gagné SM, Li MX, Sykes BD. Dynamics and thermodynamics of the regulatory domain of human cardiac troponin C in the Apo- and calcium-saturated states. *Biochemistry*. 1998;37(51):18032–44. <https://doi.org/10.1021/bi9816960>
- Szebenyi DM, Moffat K. The refined structure of vitamin D-dependent calcium-binding protein from bovine intestine. Molecular details, ion binding, and implications for the structure of other calcium-binding proteins. *J Biol Chem*. 1986;261(19):8761–77. [https://doi.org/10.1016/S0021-9258\(19\)84447-2](https://doi.org/10.1016/S0021-9258(19)84447-2)
- Wang Q, Aleshintsev A, Bolton D, Zhuang J, Brenowitz M, Gupta R. Ca(II) and Zn(II) cooperate to modulate the structure and self-assembly of S100A12. *Biochemistry*. 2019;58(17):2269–81. <https://doi.org/10.1021/acs.biochem.9b00123>
- Wang Q, Aleshintsev A, Jose AN, Aramini JM, Gupta R. Calcium regulates S100A12 zinc sequestration by limiting structural variations. *Chembiochem*. 2020;21(9):1372–82. <https://doi.org/10.1002/cbic.201900623>
- Wang Q, Kuci D, Bhattacharya S, Hadden-Perilla JA, Gupta R. Dynamic regulation of Zn(II) sequestration by calgranulin C. *Protein Sci*. 2022;31(9):e4403. <https://doi.org/10.1002/pro.4403>
- Westerlund AM, Delemotte L. Effect of Ca²⁺ on the promiscuous target-protein binding of calmodulin. *PLoS Comput Biol*. 2018;14(4):e1006072. <https://doi.org/10.1371/journal.pcbi.1006072>
- Wheeler LC, Harms MJ. Were ancestral proteins less specific? *Mol Biol Evol*. 2021;38(6):2227–39. <https://doi.org/10.1093/molbev/msab019>
- Wimberly B, Thulin E, Chazin WJ. Characterization of the N-terminal half-saturated state of calbindin D9k: NMR studies of the N56A mutant. *Protein Sci*. 1995;4(6):1045–55. <https://doi.org/10.1002/pro.5560040603>
- Wright NT, Cannon BR, Wilder PT, Morgan MT, Varney KM, Zimmer DB, et al. Solution structure of S100A1 bound to the CapZ peptide (TRTK12). *J Mol Biol*. 2009;386(5):1265–77. <https://doi.org/10.1016/j.jmb.2009.01.022>
- Wright NT, Varney KM, Ellis KC, Markowitz J, Gitti RK, Zimmer DB, et al. The three-dimensional solution structure of Ca²⁺-bound S100A1 as determined by NMR spectroscopy. *J Mol Biol*. 2005;353(2):410–26. <https://doi.org/10.1016/j.jmb.2005.08.027>
- Xie J, Burz DS, He W, Bronstein IB, Lednev I, Shekhtman A. Hexameric calgranulin C (S100A12) binds to the receptor for advanced glycated end products (RAGE) using symmetric hydrophobic target-binding patches. *J Biol Chem*. 2007;282(6):4218–31. <https://doi.org/10.1074/jbc.M608888200>
- Yang D, Mok Y-K, Forman-Kay JD, Farrow NA, Kay LE. Contributions to protein entropy and heat capacity from bond vector motions measured by NMR spin relaxation. *J Mol Biol*. 1997;272(5):790–804. <https://doi.org/10.1006/jmbi.1997.1285>
- Young BD, Cook ME, Costabile BK, Samanta R, Zhuang X, Sevdalis SE, et al. Binding and functional folding (BFF): a physiological framework for studying biomolecular interactions and allosteric. *J Mol Biol*. 2022;434(23):167872. <https://doi.org/10.1016/j.jmb.2022.167872>
- Zackular JP, Chazin WJ, Skaar EP. Nutritional immunity: S100 proteins at the host-pathogen interface. *J Biol Chem*. 2015;290(31):18991–8. <https://doi.org/10.1074/jbc.R115.645085>
- Zhang P, Tripathi S, Trinh H, Cheung MS. Opposing intermolecular tuning of Ca²⁺ affinity for calmodulin by neurogranin and CaMKII peptides. *Biophys J*. 2017;112(6):1105–19. <https://doi.org/10.1016/j.bpj.2017.01.020>
- Zimmer DB, Weber DJ. The calcium-dependent interaction of S100B with its protein targets. *Cardiovasc Psychiatry Neurol*. 2010;2010:1–17. <https://doi.org/10.1155/2010/728052>

SUPPORTING INFORMATION

Additional supporting information can be found online in the Supporting Information section at the end of this article.

How to cite this article: Wang Q, DiForte C, Aleshintsev A, Elci G, Bhattacharya S, Bongiorno A, et al. Calcium mediated static and dynamic allostericity in S100A12: Implications for target recognition by S100 proteins. *Protein Science*. 2024;33(4):e4955. <https://doi.org/10.1002/pro.4955>